Universal Features of the Topological Bond Properties of the Electron Density

Aurora Costales,* M. A. Blanco, A. Martín Pendás, Paula Mori-Sánchez,† and Víctor Luaña

Departamento de Química Física y Analítica, Facultad de Quımica, Universidad de Oviedo, 33006-Oviedo, Spain

Received: November 27, 2003; In Final Form: February 2, 2004

Every pair of atoms can be bonded together showing a variety of different bonding regimes, the internuclear distance being the controlling parameter that decides under which chemical pattern a given pair will act. The type of bond that best describes a given compound is thus a consequence of the equilibrium distances on its main atomic pairs. Therefore, we should act cautiously in extrapolating the typical molecular regime to material science, particularly when high pressures or far from room temperatures are involved.

I. Introduction

The concept of chemical bond is one of the main pieces of the chemical language. It summarizes our knowledge about the structure, geometry, stability, and reactivity of substances. Being one of the cornerstones of chemistry, it has logically suffered conceptual shifts as it became more and more systematized: from an unknown force of nature gluing the atoms in a molecule to a kind of geometrical object with little relationship to binding or cohesion. The currently dominating paradigm is based upon the ideas proposed by Pauling[1] and extended by many others and is heavily rooted in the orbital model. However, besides being not observable, the orbital description, and thus all bonding models based on it, is not invariant under the transformation laws of quantum mechanics.

The theory of Atoms in Molecules (AIM) of Bader et al.[2] surmounts these problems by proposing a description of the chemical bond that is invariant under the symmetry laws of the problem. By focusing on the electron density as a fundamental observable object, the theory recovers the image of atoms and functional groups of chemistry as regions of space, even though these regions are now completely determined by the quantum mechanics of subsystems.

The AIM theory identifies the structural elements of chemistry, bonds, rings, molecular graphs, etc., with the characteristics of the critical points of the gradient field of the electron density, $\vec{\nabla}\rho$. Other scalars constructed from ρ, like the Laplacian, $\nabla^2\rho$, complement the picture.

Soon after the initial AIM ideas were proposed, it was recognized that the Laplacian in free atoms was intimately linked to the traditional atomic shell structure.[3,4] A shell is signaled by an outer region of charge depletion ($\nabla^2\rho > 0$) followed by an inner region of charge accumulation ($\nabla^2\rho < 0$). An exam of the behavior of the Laplacian in molecules evidences how the valence shells distort upon bond formation and gives theoretical support to the valence shell electron pair repulsion model (VSEPR) of Gillespie[3,5,6] by showing how closely the charge accumulation regions are in correspondence to the bonded and lone pairs of the VSEPR model. A thorough investigation of this scalar field has also been used in a wider context to redefine acidity in terms of the balance between kinetic and potential energy densities,[7] to propose a complementary principle useful in the study of the nucleophilic and electrophilic attacks,[8] to predict sites of protonation[9] and in a wealth of other applications in chemical reactivity.

A large amount of knowledge about the behavior of the valence shells has been recorded since these ideas were introduced. However, most of it is limited to the equilibrium configurations of isolated molecules or to reaction pathways in supermolecules. Little is known about the evolution of topologies, densities, and Laplacians at far from equilibrium molecular geometries. This fact has obvious origins, for chemists do not observe easily systems frozen at such exotic geometries. After all, our world is one at near room pressure and temperature.

The development of very high pressure techniques is changing quickly this landscape. We are starting to have experimental access to unexplored regions of internuclear distance regimes where the interaction between inner atomic shells cannot be neglected. In these circumstances, our intuitions about the chemical behavior of substances, based on valence shell interactions, break, and new chemistry is expected to arise. Some examples have been already found, like the unexpected dimerization of lithium at very high pressures,[10,11] the polymerization of CO_2 to form a three-dimensional network,[12] or the predicted break of the triple bond in N_2 as pressure is increased.[13] This is just the tip of an iceberg in front of us awaiting exploration.[14]

It should be clear, in the light of these considerations, the importance of acquiring a global perspective on the bonding behavior, overcoming the artificial constraint posed by the small geometrical window that corresponds to the equilibrium geometry of a small set of molecules. One of the most interesting conclusions of this window-opening is the observation that the electron density around a bond mimics closely the superposition of the free atomic densities (i.e., the promolecular model) to zero order[15,16] or the electron density of the corresponding diatomic to first order.[17]

In addition, the work by several groups, including ours, has provided strong evidence that both the electron density and its Laplacian at bond critical points exhibit a clear exponential behavior if expressed as a function of the internuclear distance.[17−28] This was first exploited by Boyd et al. in the definition of group electronegativities on organic molecules,[18−20] even though the range of distances involved in these seminal

† Current address: Department of Chemistry, Duke University, Box 90354, Durham, NC 27708-0354.

* Corresponding author. E-mail: yoyi@carbono.quimica.uniovi.es.

10.1021/jp037627z CCC: $27.50
Published on Web 03/16/2004

studies was still rather limited. Espinosa et al. demonstrated the exponential behavior of the bond density for molecular crystals containing hydrogen bonds.[21,22,29] We have extended these results to a large variety of crystals and molecular clusters.[17,24−28] We have shown, for instance, that ionic bonds in highly ionic crystals display properties in complete parallelism to those known in covalently bonded crystals and molecules.[24,27] Furthermore, we have proved that unusual bonding phenomena, like the existence of nonnuclear maxima (NNM) of the electron density[17] or the inversion of bond polarity upon compression[28] in low-heteropolarity compounds, can be rationalized as extreme aspects in the evolution of chemical bonds with internuclear distance.

The aim of this work is to abound on these issues, trying to gather a number of loose facts into the seed of a universal model of the chemical bond between a given pair of atoms, valid in wide ranges of internuclear distances. As we will see, the type of interaction shown by such a pair is mainly determined by their internuclear distance, and a kind of universal bonding sequence emerges as this distance is decreased and inner atomic shells start to interact with each other.

The rest of the paper is organized as follows. Section II, will present some computational details and will show the similarity of the densities and Laplacians obtained with different quality calculations on a prototype diatomic. Section III presents evidence supporting a universal sequence of bonding regimes determined by the internuclear distance. We examine first a selection of homo- and heterodiatomic molecules and show that the main topological features of the electron density at the bond critical points can be predicted using simple models for the electron density. Section IV shows how the diatomic molecules may be used as a good model for the electron density of general molecules and crystals along internuclear lines, in such a way that the bonding sequence is qualitatively maintained in arbitrarily complex situations. Finally, in section V, we show that different bonded pairs that share a common atom can be organized into common trend laws by using the topological radius of the common atom instead of the interatomic distance as the grouping variable. Section VI ends the paper by recalling our main conclusions.

II. Computation of Electron Density Properties

The electron density is an observable, and there exist a number of experimental and theoretical schemes to obtain it, which differ in accuracy. Its general trends are, nevertheless, easily captured: the restructuration of the electron density on forming a particular molecule is small when compared to the superposition of atomic densities. Thus, methods that build upon atomic superposition like the LCAO (local combinations of atomic orbitals) procedures or the promolecular models will succeed in predicting the qualitative behavior of the electron density. This is not only analogous but also related to what happens with the energy: while the total energy is basically the sum of the individual atomic energies, it is precisely the small (compared to the total energy) energy difference that accounts for the binding of the molecule. This binding energy is of course mainly determined[30] by the small deformations of ρ with respect to the atomic densities, and it is in these "fine details" where the differences between methodologies will show.

The main features of ρ will then be found even with very simple models. For instance, many atomic shell structure features are conserved on going from the atoms to the molecules. Although real shells do not interpenetrate in a rigid way, the promolecular model gives very reasonable zero-order results.

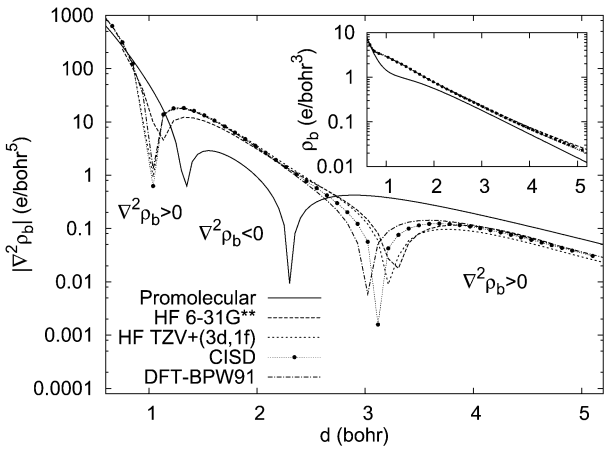

Figure 1. Promolecular, HF, CISD, and DFT-BPW91 Laplacians, $\nabla^2\rho_b$, of the electron density at the *bond critical point* of the N_2 $X-{}^1\Sigma_g^+$ ground state for a ample range of internuclear separations. The corresponding BCP electron densities are shown in the inset. Notice the logarithmic scale and the use of absolute values for the Laplacian.

To illustrate the above statements, we have plotted in Figure 1 electron densities (ρ_b in the inset) and Laplacians ($\nabla^2\rho_b$) at the *bond critical point* (BCP or bond CP) for the $X-{}^1\Sigma_g^+$ ground state of N_2. These values come from several models: (a) a promolecular model with high-quality[31] spherical atomic densities; (b) Hartree−Fock (HF) calculations using both 6-31G** and TZV+(3d,1f) basis sets as implemented in GAUSSIAN98;[32] (c) CISD (Configuration Interaction including all single and double excitations) calculations using the same TZV+(3d,1f) basis set; and (d) Generalized Gradient Approximation to Density Functional Theory (GGA-DFT) calculations using the TZV+(3d,1f) basis set with the functionals of Becke[33] and of Perdew and Wang[34] to represent the exchange and correlation contributions, respectively (BPW91).

It is readily apparent that all of the curves present the same qualitative behavior, which only deviates in a significant way from the rest in the zero-order promolecular model. This dependence indicates that the electron density at the bond critical point is mainly determined by the sum of the atomic contributions. The electron density in the bonding region may be viewed as the superposition of the atomic exponential tails. Self-Consistent-Field (SCF) and correlation effects introduce small differences, mainly in the bonding region, increasing the ρ values with respect to the promolecular ones. As the Laplacian is concerned, these effects do alter the position of the frontiers of the different bonding regimes but do not modify the qualitative description at all. It must be noted here that N_2, with its classical description as a triple-bonded diatomic, is perhaps the worst-case scenario, with one of the largest charge buildups in the covalent bonding region. It is remarkable that, even in this case, the promolecular model may serve as a qualitative guide, a behavior parallel and quite close to that obtained with better descriptions.

The similitude among the HF, CI, and DFT calculations is truly remarkable. It should be noticed, however, that these calculations differ in the equilibrium properties, particularly in the equilibrium geometry, thus causing an indirect effect on the density-related properties. This has often been a cause of much confusion. We have also analyzed the influence of the basis set on the electron density, finding that the use of flexible enough basis sets is far more important than the electronic calculation technique in determining the quality of topological properties.[35] These are very sensitive to basis sets when the latter are small and rigid, but they converge quickly and correctly as the quality

of the basis set increases. We can see in Figure 1 that ρ_b and $\nabla^2\rho_b$ at the HF level employing TZV$^+$** and 6-31G** (intermediate quality basis sets) are almost coincident in the short interatomic distance region.

Throughout the rest of the article, our analysis will be based on a diverse collection of electronic structure calculations of molecules and solids. The molecular calculations have been carried out with the GAUSSIAN98[32] code (HF, DFT, and CI LCAO) and its wave function analyzed using the AIMPAC suite[36] and the PROMOLDEN program.[37] Solid-state calculations have been performed with the PI7R15 (HF and DFT localized LCAO),[38] CRYSTAL98 (HF and DFT periodic LCAO),[39] and WIEN97 (DFT fpLAPW)[40] codes, and their densities were analyzed with CRITIC.[41] The results presented here will only include a small subset of the whole ranges of computational levels and compounds studied. They have been selected as representatives of the global behavior and span a wide range of bonding types.

III. Universal Behavior of the Shell Structure of Diatomics

In this section, we will show how the preservation of the atomic shells in molecules leads to a certain kind of universal behavior in diatomics. To do so, we will first describe the evolution of the topological properties of a representative molecule, N_2, with the interatomic distance. Later on, we will compare this behavior with that of other homo- and heterodiatomics, spanning a wide range of chemical bond types, and we will explain how these behavior is related to the atomic shell structure.

Let us examine the evolution of the bond critical point properties with the internuclear distance, taking the $X-{}^1\Sigma_g^+$ ground state of the N_2 molecule depicted in Figure 1 as a representative example. The most prominent feature of ρ_b is its exponential decay for a wide range of distances. This is a general trend for many molecules; it shows that the electron density at the bond critical point is mainly determined by the sum of the atomic contributions, and in a general sense, the promolecular approximation is valid.[27]

The BCP Laplacian also behaves exponentially over smaller segment ranges, but its structure is more complex due to the sign changes associated with the atomic shell structure.[3,4] These sign changes appear as asymptotic peaks in a logarithmic representation of $|\nabla^2\rho_b|$. The value of $\nabla^2\rho(\vec{r})$ provides a local measure of the charge density accumulation at $\vec{r}$. Accordingly, the actual sign of the Laplacian at a bond CP helps classify the bonding regimes into two gross types: (a) closed-shell ones, which occur when $\nabla^2\rho(\vec{r}_{bcp}) > 0$ (depletion of density from the bonding region) and are typical in ionic compounds and long-range van der Waals interactions, and (b) shared-shell regimes, which appear when $\nabla^2\rho(\vec{r}_{bcp}) < 0$ (concentration of electronic charge in the bonding region) and are usually found in covalent compounds. Thus, the N_2 molecule passes from a regime of closed-shell bonding for internuclear distances $d > 3$ bohr, to a typical shared-shell regime for $3 > d > 1$ bohr (which includes the equilibrium distance), and again to a closed-shell regime when $d < 1$ bohr.

These different electron density arrangements can be distinguished in Figure 2, where the Laplacian isosurfaces from CISD calculations are plotted on a plane that contains both N nuclei. At long distances, we can appreciate a deformation of the spherical atomic shells due to the still small interaction between both atoms. The Laplacian is positive at the bond CP, and the charge depleted from the internuclear region is accumulated in the rear part of the atoms. When the internuclear distance decreases, the atomic shells fuse, giving rise to a shared valence shell surrounding the atoms, with a high charge accumulation in the interatomic region, which causes the BCP Laplacian to be negative. At an interatomic distances around 1.4 bohr a new phenomenon appears, and whereas the shared valence shell is maintained, the system fulfills the necessary conditions to form a nonnuclear maximum between the two nuclei. The experimental and theoretical evidences related to these nonnuclear maxima have been repeatedly discussed, and a short review can be found in refs 17, 42, and 43. At even shorter distances, the valence shells of both atoms fuse together. Bonding is now dominated by the polarization of the inner electronic shells, thus giving place to a new regime of closed-shell interaction.

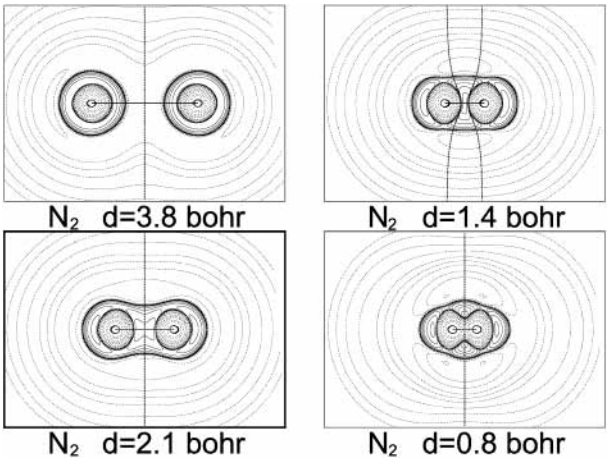

Figure 2. CISD/6-31G** Laplacian of the electron density (thin lines), bond lines (solid thick lines), and atomic surfaces (dotted thick lines) for the N_2 molecule for different interatomic distances. The thick frame indicates the equilibrium distance. Solid and dotted contours correspond to negative and positive Laplacian values, respectively. Isolines span a logarithmic scale with 38 lines in the range $10^{-3} < |\nabla^2\rho| < 10^3$ au.

The sequence of bonding regimes observed in the N_2 molecule is, in fact, general of the homodiatomic molecules. The Laplacians of Na_2 and Ne_2, represented in Figure 3, provide two further examples. We can see that, on decreasing the interatomic distance, the bonding properties follow the very same sequence for the three molecules: closed-shell, shared-shell, eventually nonnuclear maxima, and again closed-shell as the inner shells start to dominate the interaction. The three molecules, however, differ completely on the distances at which each regime occurs and even more on the actual regime shown when compared only at their respective equilibrium distance: N_2 equilibrium (2.090 bohr) lies well within the shared-shell bonding region; Na_2 (5.978 bohr) and Ne_2 (4.923 bohr) present a long equilibrium distance which causes the bond density and its Laplacian to be close to zero but within the shared-shell bonding region in the case of Na_2 and within the closed-shell region in the case of Ne_2.

It would be simple to disregard the actual importance of bonding properties at distances far from equilibrium. However, as it is going to be discussed in the next section, the electron density of the diatomic molecule serves as a good model for the behavior of the actual electron density of polyatomic molecules and solids along the interatomic lines. Nature provides then access to a wide range of interatomic distances, particularly when the effect of pressure in the solid state is considered.

The coincidence in the bonding behavior of the above three molecules is not a proof of general behavior. Henceforth, it is relevant that these phenomena can be interpreted as a conse-

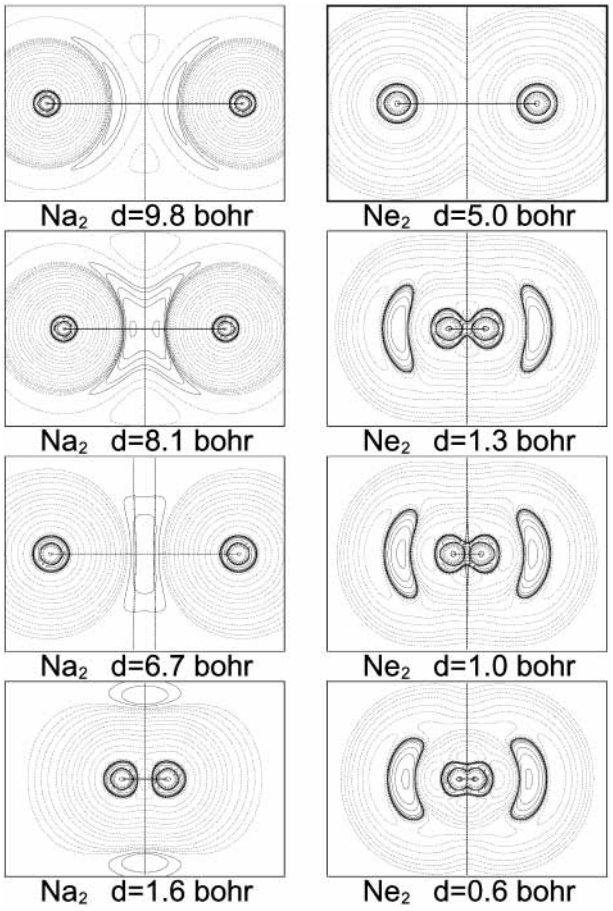

Figure 3. CISD/6-31G** Laplacian of the electron density (thin lines), bond lines (solid thick lines), and atomic surfaces (dotted thick lines) for Na_2 and Ne_2 molecules for different interatomic distances. The thick frame indicates the equilibrium distance. Isolines span a logarithmic scale with 38 lines in the range $10^{-3} < |\nabla^2\rho| < 10^3$ au.

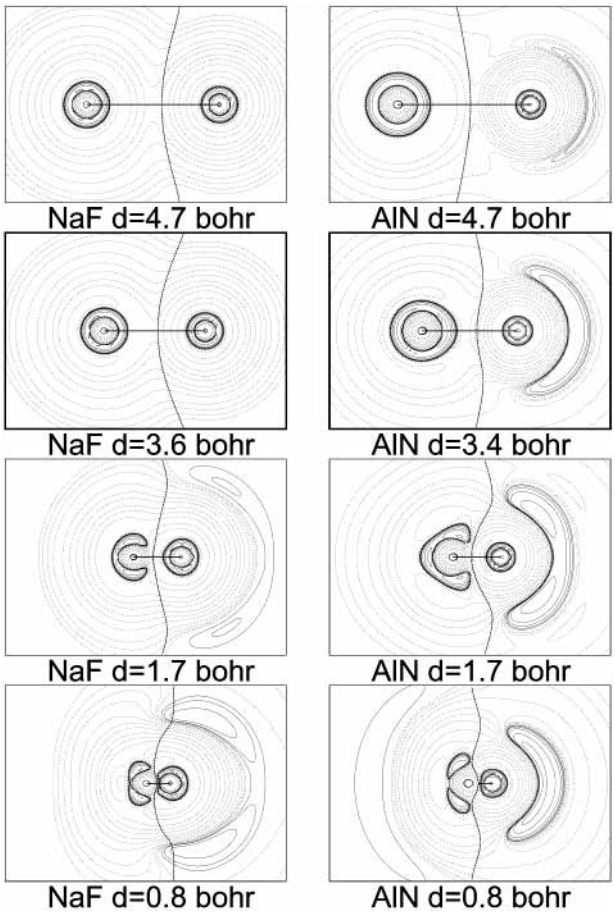

Figure 4. CISD/6-31G** Laplacian plot for the NaF and AlN molecules at different interatomics distances. Fluorine and nitrogen atoms are located at the left of their respective images. Each figure contains the isocontours of the electron density Laplacian (thin lines), bond path lines (solid thick lines), and interatomic surfaces (dotted thick lines). The thick frame indicates the equilibrium distance. Isolines span a logarithmic scale with 38 lines in the range$10^{-3} < |\nabla^2\rho| < 10^3$ au.

quence of the shell structure in the spherical atomic densities. To this end, let us consider the outcome of a promolecular model of the electron density in the homodiatomic molecule A_2. When evaluated at the midpoint between both nuclei, a critical point enforced by symmetry and usually a bond CP, the curvatures and Laplacian are

$$\rho_{\parallel}'' = 2\rho_A''(r_A) \tag{1}$$

$$\rho_{\perp}'' = 2\rho_A'(r_A)/r_A \tag{2}$$

$$\nabla^2\rho = \rho_{\parallel}'' + 2\rho_{\perp}'' = 2\rho_A''(r_A) + 4\rho_A'(r_A)/r_A \tag{3}$$

where $\parallel$ and $\perp$ represent the parallel and perpendicular directions to the A−A line, respectively; ρ_A' is the first and ρ_A'' the second radial derivative of the electron density of the atom A; and r_A is the distance from the A nucleus to the midpoint. For all atoms $\rho_A' < 0$ because atomic densities always decay when increasing the distance to the nuclear attractor. The sign of $\nabla^2\rho$ is mainly dependent on the balance between ρ_A'' and ρ_A'. At long distances, the first term is dominant, and since the tails of atomic densities are convex, $\nabla^2\rho_b$ is positive. When the interatomic distance decreases, the importance of the first radial derivative increases, giving rise to an interval in which $\nabla^2\rho_b$ is negative. This effect is enhanced in some atoms by a convex region in the radial decay of the electron density, i.e., a region in which $\rho_A'' < 0$. This accounts for nonnuclear maxima[17] because the three curvatures are now negative. If the compression continues, it is possible to access again to a range of distances in which the $\nabla^2\rho_b$ is positive because the atomic shells become interpenetrated. In this case, the dominant term is again the second radial curvature, now corresponding to the inner electronic shell of the atom. As this shell organization of the atomic density is a direct consequence of Pauli's principle and is only slightly modified from atom to atom, the analysis of the promolecular model leads us to conclude that the sequence found on N_2, Na_2, and Ne_2 should be general among the homodiatomic molecules.

Let us explore now how this image changes on considering heterodiatomic cases. It is easy to recognize that they should follow the homodiatomic behavior when the two atoms are of comparable electronegativities, so we will examine instead two examples in which the bonded atoms are unequivocally different. Our first example is NaF, traditionally classified as an ionic compound. The chemical image that we can extract from the Laplacian map represented in Figure 4 is analogous to that of the homonuclear molecules at long and at short distances. A different behavior occurs, however, around the equilibrium distance region: in this case, the atomic shells are never fused. The difference is due to the large charge transfer from the sodium to the fluorine atom. The sodium atom, in fact, loses the M valence shell, so both atoms exhibit only two atomic shells. This is the most typical feature of an ionic closed-shell interaction. Our second example is the AlN molecule, also

represented in Figure 4. The atoms in this molecule present a high electronegativity difference that induces a significant charge transfer from the electropositive (Al) to the electronegative (N) atom. However, the electronegativity difference is not large enough for Al to lose its valence shell, contrary to what happened with Na in NaF, but it induces a strong deformation of the spherical shape of the atomic shells. Molecules like AlN are best referred to as polar compounds.

The promolecular model may help us now understand the behavior of heterodiatomic molecules, AB. The interatomic midpoint is no longer fixed by symmetry to be a critical point, but rather the bond CP occurs at the internuclear position in which the two atomic densities match in slope: $\rho_A'(r_A) = \rho_B'(r_B)$, where ρ_A and ρ_B are the A and B atomic densities, respectively, and r_A and r_B are the distances from the bond CP to the atoms A and B. The Laplacian is given by $\nabla^2\rho_b = \rho_A''(r_A) + \rho_B''(r_B) + 2\rho_A'(r_A)/r_A + 2\rho_B'(r_B)/r_B$. Therefore, we have more degrees of freedom than in the homodiatomic case, but it is easy to recognize that the regimes dominated by the atomic curvatures (and thus $\nabla^2\rho_b > 0$) or by the slopes (producing $\nabla^2\rho_b < 0$) can also occur on the heteroatomic compounds. In addition, the atomic density slope at the valence tail is related to the atom's electronegativity.[27] Hence, in the case of two atoms, A and B, of identical electronegativity, the bond CP should appear at the interatomic midpoint, and the topological properties of AB would approach those of a homodiatomic system. However, if the atomic electronegativities are different, the AB diatomic molecule develops a behavior proper of ionic systems in which the valence shells are transferred totally or partially without actually fusing and are strongly deformed as a consequence of polarization.

We can conclude, from the previous analysis, that any given pair of atoms may present different bonding regimes: closed- and shared-shell bonding in particular. The interatomic distance is the magnitude that controls the bonding type actually displayed by a diatomic molecule. This explains, for example, why F_2 has a positive $\nabla^2\rho_b$. The second row diatomics N_2, O_2, F_2, and Ne_2 have increasing equilibrium distances, whereas the negative Laplacian (shared-shell) regime has a range that narrows in going from N_2 to Ne_2 (see ref 17). In the case of F_2, the equilibrium distance (2.655 bohr) is just outside of the shared-shell regime distance range (0.83−2.31 bohr), something that does not happen for the previous molecules (N_2, O_2) but does happen for the next (Ne_2).

IV. Universality of the Bond between a Pair of Atoms

Our analysis on the distance evolution of bonding in diatomics remains useful in general molecules and crystals. To show this, we examine, for instance, the C−C bonding pair in a collection of systems, spanning a wide range of C−C interatomic distances, and compare its properties to those of the C_2 diatomic molecule. We include molecules containing single (ethane), double (ethylene), and triple (acetylene) C−C bonds, aromatic molecules (benzene, anthracene), and alene, plus the diamond and graphite phases of carbon and the tetragonal structure of calcium carbide, CaC_2(II). All the molecules have been examined at their respective equilibrium geometries using a standard B3LYP/6-311G(3df,p) calculation as implemented in the GAUSSIAN98 code.[32] All crystals have been calculated at the DFT/GGA level with the Perdew−Burke−Ernzerhof exchange and correlation functional,[44] using the full potential Linear Augmented Plane Wave (fpLAPW) technique implemented in the WIEN97 code.[40] CaC_2 has been examined at the experimental geometry under room pressure and temperature (RPT).[45] Graphite has been calculated in a volume spanning 75−150% of the experimental RPT volume, and similarly, a range of 55−300% of the experimental RPT volume has been explored in diamond.

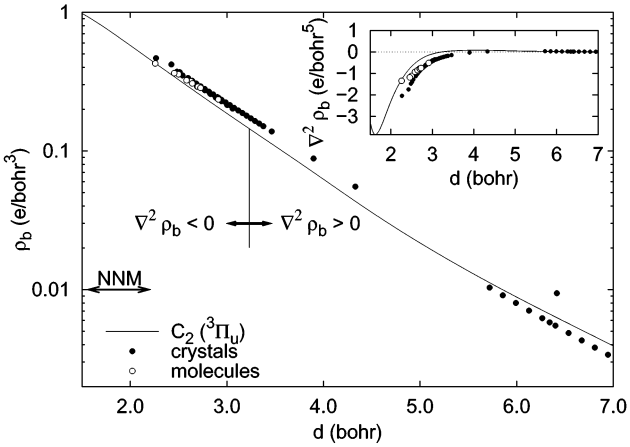

Figure 5. C−C bond density and Laplacian (inset) for a collection of molecules (open circles) and crystals (solid circles) described in the main text. The properties of the $^3\Pi_u$ state of the C_2 diatomic molecule are also represented (solid line) for comparison. The vertical lines indicate the changes in the nature of the bonding.

Figure 5 presents a graphical comparison of the ρ_b and $\nabla^2\rho_b$ values for all the systems described above. The range of C−C distances is quite large, 2−7 bohr, the largest values corresponding to the interplanar bonding in graphite and to the secondary bonds among C_2 groups in CaC_2. This makes even more remarkable the excellent correlation with the C−C distance that is shown by the bonding densities of all the systems. Molecular and crystal values can be fitted to

$$\rho_b = ce^{-\gamma d_{CC}}, \quad c = 5.21 \text{ e bohr}^{-3}, \quad \gamma = 1.06 \text{ bohr}^{-1} \qquad (4)$$

with a correlation coefficient of 99.8%. The agreement between molecules and crystals applies also to the bond Laplacians (see the inset in Figure 5). In addition, all systems follow the same sequence of bonding regimes. For instance, the C−C bonding remains a prototypical shared-shell interaction if the interatomic distance is less than 3.2 bohr, but it is a closed-shell interaction for larger distances.

The C_2 diatomic molecule provides a good model for the C−C bond path in any compound, as Figure 5 clearly shows. To do this comparison, we must consider a triplet electronic state of C_2 (either the $^3\Pi_u$ or the $^3\Sigma_g^-$ will serve, as their bond density and Laplacian are essentially identical), as the unpaired electrons will couple to the rest of the molecule in the larger compounds causing only a small effect on the C−C line.

The above evidence indicates clearly that the C−C bonding properties are transferable among many different molecular and crystalline systems, once the interatomic distance is taken into account. The same behavior is found when other atomic pairs are considered, and we should point to ref 24, where we have reported a similar but less exhaustive analysis of the O−O bonding. Similarly, Espinosa et al. have demonstrated that the experimental bond CP properties correlate with the bond length distance for −O···H−, −N···H−, and −F···H− hydrogen bonds,[21,22,29] a correlation also confirmed by Gálvez et al.,[46] and Mallinson et al. have shown that the inter- and intramolecular experimental bond CP properties of a collection of naphthalene derivatives follow exponential dependences on the bond length.[47] The cause for this transferability can be easily pointed out if we assume that the electron density at a given point is dominated by the contribution from the closest atoms

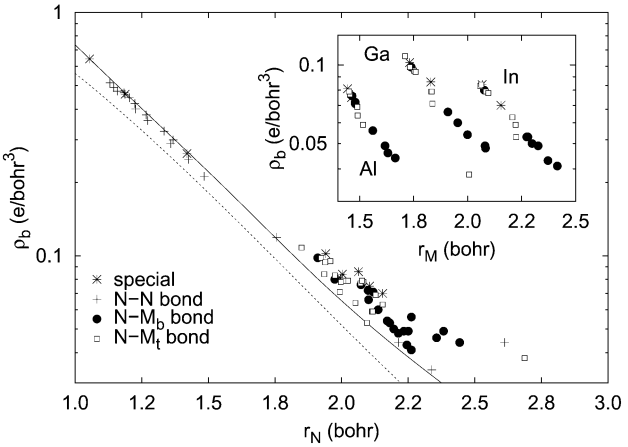

Figure 6. Logarithmic plot of the electron density at the N−N and M−N bond CP's represented versus the N bonding radius (r_N, main figure) and versus the M radius (r_M, inset). Most of the points correspond to clusters of group III nitrides, and we have distinguished between bonding to *terminal* and to *bridge* metal atoms, M_t (open squares) and M_b (dark circles), respectively. The points labeled *special* correspond to N−N bonds in a collection of reference compounds: the N_2 molecule, several N_2H_m hydrides, and the zinc blende phase (B3) of group III nitride crystals. The solid line is the electron density on the bond point of the N_2 molecule, calculated as a function of the internuclear distance, and the dotted line is the promolecular estimation of the same density. Computational details as well as a complete description of the clusters composition and geometry can be found in ref 26.

around it, as it happens within the promolecular model, and the influence of the crystalline or molecular environment is small. The correlation shown by the high-quality densities depicted in Figure 5 does not depend, however, on any crude estimation, but it should be regarded as an attribute of the density along the interatomic bond path. A significant consequence of this kind of universal behavior is the continuity in the bonding properties from the molecular to the crystalline compounds.

V. Transferability across Different Bonded Pairs

Bonding density−distance correlations such as that found in eq 1 can be obtained for any pair of atoms bonded together. It is difficult, however, to establish comparisons among pairs formed between different atoms. In our recent analysis of group III nitride clusters and crystals (MN, M = Al, Ga, and In), we have found[26] that the correlations can be extended even to different pairs of atoms when the distance from the bond point to a common atom (r_N or r_M, in this case) is employed instead of the internuclear distance. This is readily shown in Figure 6, where the bond density (ρ_b) is represented in a logarithmic scale versus r_N (main figure) and versus r_M (inset). We can see that the electron density at the M−N bond CP varies as a decreasing exponential with either the r_N or the r_M radius.

It is remarkable that Figure 6 contains data from a wide collection of compounds of very different nature: molecules containing short N−N covalent bonds like N_2 and several nitrogen hydrides; clusters containing weak M−N bonds like M_6N_2-2, M_2N_2, and M_2N_2-2 (see the description of cluster names and geometries in ref 26); and compounds containing highly polar or ionic M−N bonds like the M_6N_2 clusters or the B3 phase of the group III nitride crystals. Even though the points are more scattered in the long distance region, corresponding to heteronuclear bonds, there is a clear dependence of the bond CP electron density on the distance, not only when the same pair of atoms is involved but also when only one of the atoms (N) is common in all of the bonds. Henceforth, all compounds containing N share a common trend, revealed by plotting ρ_b versus r_N, even though we are comparing in the same plot N−Al, N−Ga, N−In, N−H, and N−N bonds. This trend would not be apparent if the interatomic M−N distances were being used. However, the common trend splits in different trends for different bonds (similar to those displayed by ρ_b versus d) when we focus in r_M, the distance from the bond point to the non-nitrogen atom (inset of Figure 6).

A simplification of the promolecular model provides now a specific prediction that justifies the above exponential trends. Let AB be the two atoms bonded and r_A the distance from A to the bond CP. The BCP will occur at the point in which the two atomic densities match in slope, $\rho_A'(r_A) = \rho_B'(r_B)$, where ρ_A' and ρ_B' are the radial derivatives. Within the *exponential tail model*[27] the radial density of an atom in the promolecule is described as a single exponential for a range of distances containing the distance to the BCP: $\rho_A(r_A) = ae^{-\alpha r_A}$. Used in the slope match condition, this provides the relationship $\alpha\rho_A(r_A) = \beta\rho_B(r_B)$. The total density at the BCP is made up of the contribution of both atoms, so

$$\rho_b^{AB}(r_A) = \rho_A(r_A) + \rho_B(r_B) = \left(1 + \frac{\alpha}{\beta}\right)\rho_A(r_A) = a\left(1 + \frac{\alpha}{\beta}\right)e^{-\alpha r_A} \quad (5)$$

If we consider the same pair AB in a collection of compounds, the decaying exponential behavior $\rho_b = Ce^{-\alpha r_A}$ is immediate and will resemble the ρ_b versus d behavior already described in section IV.

The case of different pairs AB, AC, AD, ... sharing a common atom A is more interesting. Since $\rho_b^{AA}(r_A) = 2\rho_A(r_A)$, we can rewrite eq 5 as $\rho_b^{AB}(r_A) = (1 + \alpha/\beta)\rho_b^{AA}(r_A)/2$ or, equivalently, $\rho_b^{AB}(r_B) = (1 + \beta/\alpha)\rho_b^{BB}(r_B)/2$: ρ_b^{AB} has the same behavior of the homodiatomics modulated by the α/β ratio. If we consider C, D, ... instead of B, we will have the α/γ, α/δ, ... ratios instead of the α/β ratio. To estimate the variation in the logarithmic plot upon modification of β, we substitute $(1 + \alpha/\beta)/2$ by $(1 + (\alpha - \beta)/2\beta)$ and Taylor-expand the logarithm up to first order

$$\ln \rho_b^{AB}(r_A) = \ln \rho_b^{AA}(r_A) + \ln\left(1 + \frac{\alpha - \beta}{2\beta}\right) \simeq \ln \rho_b^{AA}(r_A) + \frac{\alpha - \beta}{2\beta} \quad (6)$$

Thus, according to the exponential tail model, the AB molecules will deviate from the AA diatomic exponential behavior by a constant, half of the relative deviation of the exponents. This would be obviously smaller, and thus the different trends closer, when either $\alpha \ll \beta$ or $\alpha \simeq \beta$. Unfortunately, the exponent of the nitrogen atom is larger (2.70 bohr^{-1}, obtained from a calculation on the N_2 molecule) and not smaller than those of the group III metal atoms: 1.42, 1.96, and 1.82 bohr^{-1} for Al, Ga, and In, respectively. Using these numbers, we should expect deviations within the 10−20 range, as Figure 6 readily shows. Ga and In nitrides, on the other hand, are expected to behave quite similarly, since their $(\alpha - \beta)/2\beta$ values are very similar on a logarithmic scale.

The bond density Laplacians for the group III nitride clusters and crystals, depicted in Figure 7, behave similarly to the bonding densities, as we have already shown in ref 25. However, in this case the exponential trends are different for each type of bond. In a way this is not unexpected because $\nabla^2\rho_b$ is closely linked to the character of the chemical bond.[2] On the other hand,

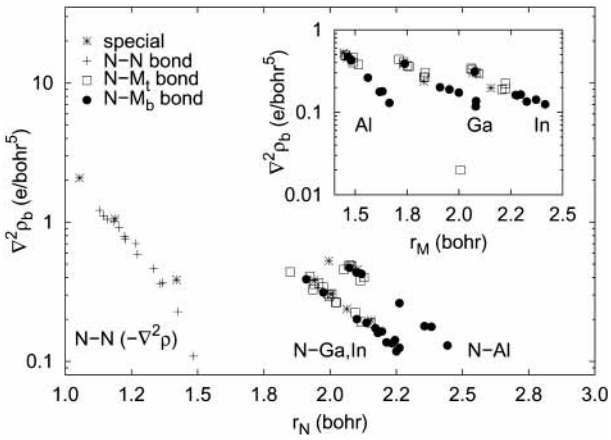

Figure 7. Logarithmic plot of the Laplacian of the electron density at the bond CP versus the r_N (main figure) and r_M (inset) topological radii. Labels as in Figure 6. In the case of N−N bonds, most of which have negative Laplacians, $-\nabla^2\rho$ is depicted, and bonds with positive Laplacians have been omitted.

the promolecular with exponential tails model predicts for an AB pair

$$\nabla^2\rho_b{}^{AB}(r_A) = \left(1 + \frac{\beta - 2/r_B}{\alpha - 2/r_A}\right)\nabla^2\rho_A(r_A) \qquad (7)$$

Clearly, the behavior of the Laplacian is more complex than that of the density, but we can still relate it to the behavior of the homodiatomic

$$\nabla^2\rho_b{}^{AB}(r_A) = \frac{1}{2}\left(1 + \frac{\beta - 2/r_B}{\alpha - 2/r_A}\right)\nabla^2\rho_b{}^{AA}(r_A) \qquad (8)$$

If we again Taylor-expand the logarithmic dependence, we get

$$\ln \nabla^2\rho_b{}^{AB}(r_A) \simeq \ln \nabla^2\rho_b{}^{AA}(r_A) + \frac{(\beta - 2/r_B) - (\alpha - 2/r_A)}{2(\alpha - 2/r_A)} \qquad (9)$$

again half a relative deviation, in this case of the $\alpha - 2/r_A$ magnitudes. Since this does depend on the distances to both atoms, the trend will not be a single exponential as in the ln $\rho_b{}^{AB}$ case. Given the typical sizes of the atoms in this range ($r_N \in [1.9, 2.4]$, $r_{Al} \in [1.5, 1.8]$, $r_{Ga} \in [1.8, 2.1]$, $r_{In} \in [2.1, 2.4]$, all values in bohr), we could expect wide variations in the relative deviation. However, the relative deviations of Ga and In are quite similar, since although $\alpha_{Ga} > \alpha_{In}$ and $r_{Ga} < r_{In}$, $\alpha_{Ga} - 2/r_{Ga} \simeq \alpha_{In} - 2/r_{In}$, and thus their curves almost overlap in Figure 7. Notice, however, that this only happens when employing r_N, and thus the deviation occurs with respect to a common $\nabla^2\rho_b{}^{NN}$ curve; the inset shows that the curves for r_{Ga} and r_{In} are quite different, since $\nabla^2\rho_b{}^{GaGa}$ and $\nabla^2\rho_b{}^{InIn}$ are quite different.

As mentioned in section II, the deviation of the actual density from that of the promolecular model is a measure of the binding energy of the system. The first theorem of Hohenberg and Kohn[30] warrants that the knowledge of the density suffices to access the energy. The bond path, in general, and the bond critical point, in particular, are regions of maximal density changes with respect to the promolecular situation. This means that the systematic study of the differences between promolecular and actual densities at BCP's may uncover clues about the nature of the universal density functional. Further work is clearly needed along these lines.

VI. Conclusions

Some general conclusions can be extracted from our analysis of atomic pairs in diatomic and polyatomic molecules, clusters, and crystals. First, a given pair of atoms follows a universal sequence of bonding regimes which is entirely controlled by the interatomic distance. This behavior is easily captured with any density model built from atomic contributions, and it is caused by the intrinsic electronic shell structure of atoms, which is largely conserved in general compounds. Second, the actual sequence goes as follows: closed-shell bonding is typical of large internuclear separations and, as the two atoms approach, a shared-shell regime appears; then nonnuclear maxima can occur in some cases, up to the moment that the inner shells of the atoms start to interact, and the cycle starts again with a closed-shell regime. Third, diatomic molecules serve well to predict the behavior of a bonding pair of atoms in a larger molecular or crystalline environment. Fourth, the promolecular model and, to a lesser extent, its exponential tails simplification provide specific predictions for the bond CP electron density and Laplacian that agree qualitatively and explain the trends actually observed on state-of-the-art quantum mechanical calculations. For instance, the electron density at an internuclear bond CP decays exponentially with the bonding distance and also with the distance from the bond CP to any of the bonded atoms. This last dependence is also shown to be true even for bonds of different atoms to a single one, provided that the distance to the common atom is used. The absolute value of the Laplacian at the bond CP usually decays exponentially, but this trend may fail under appropriate circumstances.

Acknowledgment. This research has been funded by the Spanish Ministerio de Ciencia y Tecnología, Grants BQU2000-0466 and BQU2003-06553. A.C. thanks the Spanish Ministerio de Ciencia y Tecnología for her Ramón y Cajal position. P.M.S. is currently a Fulbright fellow.

References and Notes

(1) Pauling, L. *The Nature of the Chemical Bond;* Cornell University Press: Ithaca, NY, 1960.

(2) Bader, R. F. W. *Atoms in Molecules;* Oxford University Press: Oxford, 1990.

(3) Bader, R. F. W.; Gillespie, R. J.; Macdougall, P. J. *J. Am. Chem. Soc.* **1988**, *110*, 7329−7336.

(4) Shi, Z.; Boyd, R. J. *J. Chem. Phys.* **1988**, *88*, 4375−4377.

(5) Gillespie, R. J. *Struct. Chem.* **1998**, *9*, 73−76.

(6) Gillespie, R. J. *Coord. Chem. Rev.* **2000**, *197*, 51−69.

(7) Bader, R. F. W.; MacDougall, P. J. *J. Am. Chem. Soc.* **1985**, *107*, 6788−6795.

(8) Carroll, M. T.; Cheeseman, J. R.; Osman, R.; Weinstein, H. *J. Phys. Chem.* **1989**, *93*, 5120−5123.

(9) Bader, R. F. W.; Chang, C. *J. Phys. Chem.* **1989**, *93*, 2946−2956.

(10) Neaton, J. B.; Ashcroft, N. W. *Nature (London)* **1999**, *400*, 141−144.

(11) Ashcroft, N. W. *Nature (London)* **2002**, *419*, 569−571.

(12) Iota, V.; Yoo, C. S.; Cynn, H. *Science* **1999**, *283*, 1510−1513.

(13) Eremets, M. I.; Hemley, R. J.; Mao, H.-K.; Gregoryanz, E. *Nature (London)* **2001**, *411*, 170−174.

(14) Hemley, R. J. *Annu. Rev. Phys. Chem.* **2000**, *51*, 763−800.

(15) Spackman, M.; Maslen, E. N. *Acta Crystallogr. A* **1984**, *40*, C172−C172.

(16) Spackman, M. A.; Maslen, E. N. *J. Phys. Chem.* **1986**, *90*, 2020−2027.

(17) Martín Pendás, A.; Blanco, M. A.; Costales, A.; Mori-Sánchez, P.; Luaña, V. *Phys. Rev. Lett.* **1999**, *83*, 1930−32.

(18) Boyd, R. J.; Edgecombe, K. E. *J. Am. Chem. Soc.* **1988**, *110*, 4182−4186.

(19) Boyd, R. J.; Boyd, S. L. *J. Am. Chem. Soc.* **1992**, *114*, 1652−1655.

(20) Komorowski, L.; Boyd, S. L.; Boyd, R. J. *J. Phys. Chem.* **1996**, *100*, 3448−3453.
(21) Espinosa, E.; Molins, E.; Lecomte, C. *Chem. Phys. Lett.* **1998**, *285*, 170−173.
(22) Espinosa, E.; Souhassou, M.; Lachekar, H.; Lecomte, C. *Acta Crystallogr. B* **1999**, *55*, 563−572.
(23) Downs, R. T.; Gibbs, G. V.; Boisen, M. B., Jr.; Rosso, K. M. *Phys. Chem. Minerals* **2002**, *29*, 369−385.
(24) Luaña, V.; Costales, A.; Mori-Sánchez, P.; Martín Pendás, A. *J. Phys. Chem. B* **2003**, *107*, 4912−4921.
(25) Costales, A.; Kandalam, A. K.; Martín Pendás, A.; Blanco, M. A.; Recio, J. M.; Pandey, R. *J. Phys. Chem. B* **2000**, *104*, 4368.
(26) Costales, A.; Blanco, M. A.; Martín Pendás, A.; Kandalam, A. K.; Pandey, R. *J. Am. Chem. Soc.* **2002**, *124*, 4116−23.
(27) Martín Pendás, A.; Costales, A.; Luaña, V. *J. Phys. Chem. B* **1998**, *102*, 6937−6948.
(28) Mori-Sánchez, P.; Martín Pendás, A.; Luaña, V. *Phys. Rev. B* **2001**, *63*, 125103−1−4.
(29) Espinosa, E.; Alkorta, I.; Elguero, J.; Molins, E. *J. Chem. Phys.* **2002**, *117*, 5529−5542.
(30) Hohenberg, P.; Kohn, W. *Phys. Rev. A* **1964**, *136*, B864.
(31) Koga, T.; Watanabe, S.; Kanyayama, K.; Yasuda, R.; Thakkar, A. J. *J. Chem. Phys.* **1995**, *103*, 3000.
(32) Frisch, M.; Trucks, G. W.; Schlegel, H. B.; Scuseria, G. E.; Robb, M. A.; Cheeseman, J. R.; Zakrzewski, V. G.; Montgomery, J. A.; Stratmann, R. E.; Burant, J. C.; Dapprich, S.; Millam, J. M.; Daniels, A. D.; Kudin, K. N.; Strain, M. C.; Farkas, O.; Tomasi, J.; Barone, V.; Cossi, M.; Cammi, R.; Mennucci, B.; Pomelli, C.; Adamo, C.; Clifford, S.; Ochterski, J.; Petersson, G. A.; Ayala, P. Y.; Cui, Q.; Morokuma, K.; Malick, D. K.; Rabuck, A. D.; Raghavachari, K.; Foresman, J. B.; Cioslowski, J.; Ortiz, J. V.; Stefanov, B. B.; Liu, G.; Liashenko, A.; Piskorz, P.; Komaromi, I.; Gomperts, R.; Martin, R. L.; Fox, D. J.; Keith, T.; Al-Laham, M. A.; Peng, C. Y.; Nanayakkara, A.; Gonzalez, C.; Challacombe, M.; Gill, P. M. W.; Johnson, B. G.; Chen, W.; Wong, M. W.; Andres, J. L.; Head-Gordon, M.; Replogle, E. S.; Pople, J. A. Gaussian 98: Gaussian, Inc., Pittsburgh, PA, 1998.
(33) Becke, A. D. *Phys. Rev. A* **1988**, *38*, 3098.
(34) Perdew, J. P.; Wang, Y. *Phys. Rev. B* **1992**, *45*, 13244.
(35) Francisco, E.; Costales, A.; Martín Pendás, A. *J. Phys. Chem. A* **2001**, *105*, 4126−4135.
(36) Keith, T. A.; Laidig, K. E.; Krug, P.; Cheeseman, J. R.; Bone, R. G. A.; Biegler-König, F. W.; Duke, J. A.; Tang, T.; Bader, R. F. W. The *aimpac95* programs, 1995.
(37) Promolden: a program for the topological analysis of molecular wave functions in the space and momentum representations. Martín Pendás, A., 2001−2003.
(38) Blanco, M. A.; Luaña, V.; Martín Pendás, A. *Comput. Phys. Commun.* **1997**, *103*, 287−302.
(39) Dovesi, R.; Saunders, V. R.; Roetti, C.; Causà, M.; Harrison, N. M.; Orlando, R.; Zicovich-Wilson, C. M. Crystal98 user's manual, 1998.
(40) Blaha, P.; Schwarz, K.; Luitz, J. WIEN97, a Full Potential Linearized Augmented Plane Wave package for calculating crystal properties, 1999.
(41) The critic program. Martín Pendás, A.; Luaña, V. 1995−2003.
(42) Madsen, G. K. H.; Blaha, P.; Schwarz, K. *J. Chem. Phys.* **2002**, *117*, 8030−8035.
(43) Luaña, V.; Mori-Sánchez, P.; Costales, A.; Blanco, M. A.; Martín Pendás, A. *J. Chem. Phys.* **2003**, *119*, 6341−6350.
(44) Perdew, J. P.; Burke, S.; Ernzerhof, M. *Phys. Rev. Lett.* **1996**, *77*, 3865.
(45) Atoji, M.; Medrud, R. C. *J. Chem. Phys.* **1959**, *31*, 332.
(46) Gálvez, O.; Gómez, P. C.; Pacios, L. F. *J. Chem. Phys.* **2001**, *115*, 11166−11184.
(47) Mallinson, P. R.; Smith, G. T.; Wilson, C. C.; Grech, E.; Wozniak, K. *J. Am. Chem. Soc.* **2003**, *125*, 4259−4270.